

國立交通大學
材料科學與工程學系
博士論文

錳含量對銅錳鋁合金相變化之影響



研究生：楊勝裕

指導教授：劉增豐 博士

中華民國九十五年一月

Effects of Manganese Content on the Phase Transformations of the Cu-Mn-Al Alloys

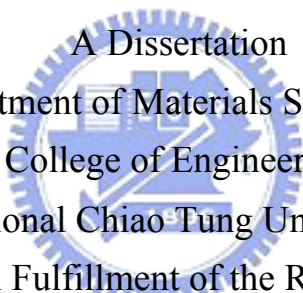
研究生：楊勝裕

Student: Chih-Hao Chen

指導教授：劉增豐 博士

Advisor: Dr. Tzeng-Feng Liu

國立交通大學
材料科學與工程學系
博士論文



A Dissertation
Submitted to Department of Materials Science and Engineering
College of Engineering
National Chiao Tung University
in Partial Fulfillment of the Requirements
for the Degree of
Doctor of Philosophy
in
Materials Science and Engineering
January 2005
Hsinchu, Taiwan, Republic of China

中華民國九十五年一月

誌 謝

由衷感謝指導教授劉增豐博士七年多來的悉心指導與諄諄教誨，使得學生的研究工作得以順利進行，並如期完成本論文。在這七年多的過程中，吾師除了在繁忙的公務中抽空指導實驗工作外，並不時引導學生如何由參考文獻中發覺問題，進而尋找論文之研究方向與解決方法，以及如何撰寫科技論文等，實是受益良多；特別是在吾師擔任工學院院長期間，校內公務日漸繁重，無法時常陪伴師母與子女左右，卻仍犧牲假日家庭時間，陪伴學生討論實驗結果、指導論文後續的研究方向，令學生感到十二萬分的敬佩。在生活上，特別感謝吾師劉增豐教授與師母林美慧老師無微不至的關懷和鼓勵，謹致以最高的敬意與誠摯的感謝。在課業上，感謝系上教授們提供良好的學習環境。口試時，承蒙賀俊教授、吳泰伯教授、莊振益教授、朝春光教授等口試委員悉心指正，更是受益匪淺。

感謝交大羽球隊教練廖威彰老師的栽培，提供良好的羽球學習環境以及球隊寒、暑假嚴苛的密集訓練，讓我不但擁有在球技上的成長更獲得充沛的體能熬夜做實驗。另外，從日常與教練的談話中體會出如何待人處世之道，是我在交大學生生涯中最難忘的一段回憶，我會永遠以曾經身為交大羽球隊的一員為榮。另外感謝球隊學長新松、仁宗、智揚、偉賓、志壕、振泓(白猴)、文億、祐生、旭正、力衡、小勇、廷彰、花輪、克彬以及其他學弟妹們多年來的照顧，感謝大家一起陪我走過這一段既艱辛又甘甜的旅途。

研究所期間，承蒙學長李堅瑋博士、陳志壕博士及鄭祥誠博士在電子顯微鏡之分析與金屬相變化上的指導，在此特別值得一提的是志壕學長，若無他的帶領進入球隊，我無法認識那麼多的好朋友。此外，就讀交大研究所期間，受到堅瑋及志壕學長許多的提攜，使我得以如此順利取得學位。感謝承舜學長、俊瑋及瑞陞學弟在論文完稿過程中實驗上的

協助，尤其是俊瑋及瑞陞學弟，在我準備論文最忙之際，慨然地幫助我打字與校稿，幫我節省了許多寶貴的時間，由衷感激。一路走來得到實驗室學長學弟一貫的相互扶持與鼓勵，讓我在研究過程中，有最溫馨的感覺。此外，國科會在研究經費上之贊助，使得本論文得以順利完成，在此一併致上衷心的謝意。

最後，僅將論文獻給我最敬愛的奶奶、父母親及心愛的老婆薇伶，感謝他們多年來的辛勞、支持與鼓勵，使我能在安定舒適的環境中順利地完成學業。特別值得一提的是老婆薇伶，她是我在交大研究所求學生涯中最大的收穫。同時也感謝關心我的岳父母、茂勝、慶潭以及其他所有親友們。



錳含量對銅錳鋁合金相變化之影響

研究生：楊勝裕

指導教授：劉增豐 博士

國立交通大學材料科學與工程研究所

中文摘要

本論文利用光學顯微鏡，掃描穿透式電子顯微鏡和X光能量散佈分析儀等，研究觀察不同之錳含量對銅-錳-鋁三元合金顯微結構組織的影響。

本論文所得到的具體研究結果如下：



(一)、在淬火狀態下， $\text{Cu}_{2.9}\text{Mn}_{0.1}\text{Al}$ (Cu-2.7at.%Mn-25.1at.%Al) 合金顯微結構為 D0_3 相與淬火過程中經由麻田散相變化轉變成 γ_1' 麻田散相之混合相。然而我們發現在淬火狀態下， $\text{Cu}_{2.8}\text{Mn}_{0.2}\text{Al}$ (Cu-5.1at.%Mn-25.3at.%Al) 與 $\text{Cu}_{2.7}\text{Mn}_{0.3}\text{Al}$ (Cu-7.6at.%Mn-25.1at.%Al) 合金，其顯微結構為 D0_3 相和極細微之L-J混合相。但是在 $\text{Cu}_{2.6}\text{Mn}_{0.4}\text{Al}$ (Cu-10.3at.%Mn-25.2at.%Al) 合金在淬火狀態下之顯微結構則變成為 D0_3 、 L2_1 與L-J之混合相，此結果與先前Bouchard等其他學者在銅-錳-鋁三元合金系統中所發現到的結果不同。在本研究中我們可清楚的觀察到 $a/4\langle 111 \rangle$ 反向晶界存在於 $\text{Cu}_{2.9}\text{Mn}_{0.1}\text{Al}$ 、 $\text{Cu}_{2.8}\text{Mn}_{0.2}\text{Al}$ 及

$\text{Cu}_{2.7}\text{Mn}_{0.3}\text{Al}$ 合金中，這是一個強而有力的直接證據證明 D0_3 相是經由 $\beta \rightarrow \text{B2} \rightarrow \text{D0}_3$ 連續規律化變態所形成的。此處特別值得一提的是，至今 $a/4\langle 111 \rangle$ 反向晶界從未被其他學者在銅-錳-鋁合金系統中發現過。

(二)、當 $\text{Cu}_{2.7}\text{Mn}_{0.3}\text{Al}$ (銅-7.6at.%錳-25.1at.%鋁) 合金在固溶處理後急速淬火後，其顯微結構為 D0_3 和極細微之 L-J 混合相，其中 D0_3 相是在淬火過程中經由 $\beta \rightarrow \text{B2} \rightarrow \text{D0}_3$ 連續規律化變態所形成的。當此合金在 500°C 做適當時間之時效處理後， γ -brass 相會開始在 D0_3 基地中沿著 $a/2\langle 100 \rangle$ 反向晶界析出。然而，隨著時效時間的增加，L-J 析出物開始在 γ -brass 顆粒周圍的鄰近區域析出，此 γ -brass 與 L-J 的共存現象至今從未被其他學者在銅-錳-鋁合金系統中發現過。此合金在 500°C 至 700°C 溫度範圍內做時效處理後其顯微結構之變化依序為： $(\gamma\text{-brass} + \text{L-J} + \text{D0}_3) \rightarrow (\gamma\text{-brass} + \text{L-J} + \text{B2}) \rightarrow \beta$ 。此結果與其他學者在 $\text{Cu}_{3-x}\text{Mn}_x\text{Al}$ 三元合金中當 $x \leq 0.32$ 時所發現到的結果截然不同。

(三)、在淬火狀態下， $\text{Cu}_{1.6}\text{Mn}_{1.4}\text{Al}$ (銅-35.1at.%錳-25.1at.%鋁) 合金的淬火顯微結構為 L2_1 、B2 與 L-J 之混合相，這個發現和其他學者在 $\text{Cu}_{3-x}\text{Mn}_x\text{Al}$ 合金 ($x \leq 1.0$) 合金中所發現到的結果不同。當此合金在 460°C 做短時間時效處理後， γ -brass 顆粒會開始在 L2_1 基地中沿著反向晶界析出。隨著時效時間的增

加， γ -brass析出物逐漸成長並且 β -Mn析出物開始在 γ -brass析出物之周圍析出， γ -brass與 β -Mn之間的方向關係為 $(001)_{\gamma\text{-brass}} // (012)_{\beta\text{-Mn}}$ and $(011)_{\gamma\text{-brass}} // (031)_{\beta\text{-Mn}}$ ，此 γ -brass與 β -Mn的共存現象至今從未被其他學者在銅-錳-鋁合金系統中發現過。此合金在 460°C 至 700°C 溫度範圍內做時效處理後其顯微結構之變化依序為： $(\gamma\text{-brass} + \beta\text{-Mn}) \rightarrow (\beta\text{-Mn} + \text{B2}) \rightarrow \beta$ 。



Effects of Manganese Content on the Phase Transformations of the Cu-Mn-Al alloys


Student: Sheng-Yu Yang

Advisor: Dr. Tzeng-Feng Liu

Department of Materials Science and Engineering

National Chao Tung University

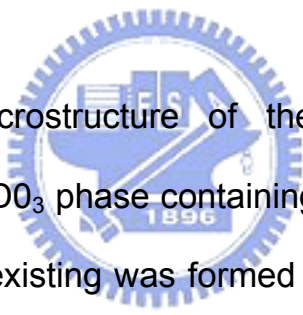
Abstract



Effects of the manganese (Mn) content on the phase transformations of the Cu-Mn-Al ternary alloys have been investigated by means of optical microscopy, scanning transmission electron microscopy and energy-dispersive X-ray spectrometry. On the basis of the experimental examinations, several results can be summarized as follows:

[1]. We have studied the $\text{Cu}_{3-x}\text{Mn}_x\text{Al}$ alloy systems at room temperature. In the as-quenched condition, the microstructure of the $\text{Cu}_{2.9}\text{Mn}_{0.1}\text{Al}$ (Cu-2.7 at.%Mn-25.1at.%Al) alloy was a mixture of ($\text{D0}_3 + \gamma_1'$ martensite) phases. However, the as-quenched microstructures of the $\text{Cu}_{2.8}\text{Mn}_{0.2}\text{Al}$ (Cu-5.1at.%Mn-25.3at.%Al) and $\text{Cu}_{2.7}\text{Mn}_{0.3}\text{Al}$ (Cu-7.6at.%Mn-25.1at.%Al) alloys were found to be D0_3 phase containing extremely fine L-J precipitates. However, as the X increasing to 0.4, that is $\text{Cu}_{2.6}\text{Mn}_{0.4}\text{Al}$

(Cu-10.3at.%Mn-25.2at.%Al) alloy, it was a mixture of ($D0_3 + L2_1 + L-J$) phases in the as-quenched condition. These results are different from those proposed by Bouchard et al. The $D0_3$ phase in the $Cu_{2.9}Mn_{0.1}Al$, $Cu_{2.8}Mn_{0.2}Al$ and $Cu_{2.7}Mn_{0.3}Al$ alloys was formed by a $\beta \rightarrow B2 \rightarrow D0_3$ continuous ordering transition during quenching, because of the presence of $a/4\langle 111 \rangle$ anti-phase boundaries (APBs). It is a strong evidence to demonstrate that the existing $D0_3$ phase was formed by a $\beta \rightarrow B2 \rightarrow D0_3$ continuous ordering transition during quenching. It is worthwhile to note here also that the $a/4\langle 111 \rangle$ APBs have never been found in the Cu-Mn-Al alloy systems before.



[2]. The as-quenched microstructure of the $Cu_{2.7}Mn_{0.3}Al$ (Cu-7.6at.%Mn-25.1at.%Al) alloy was $D0_3$ phase containing extremely fine L-J precipitates, where the $D0_3$ phase existing was formed by a $\beta \rightarrow B2 \rightarrow D0_3$ continuous ordering transition during quenching. When the as-quenched alloy was aged at $500^\circ C$ for moderate times, the γ -brass particles were found to nucleate preferentially at $a/2\langle 100 \rangle$ APBs. However, with increasing the aged times at $500^\circ C$, the L-J precipitates started to appear at the regions contiguous to the γ -brass particles. The coexistence of (γ -brass + L-J) phases has never been observed by other workers in the Cu-Mn-Al alloy systems before. As the aging temperature was increased from $500^\circ C$ to $700^\circ C$, the phase transition sequence was found to be (γ -brass + L-J + $D0_3$) \rightarrow (γ -brass + L-J + B2) \rightarrow β . This result is different from that reported by

previous workers in $\text{Cu}_{3-x}\text{Mn}_x\text{Al}$ alloys with $X \leq 0.32$.

[3]. In the as-quenched condition, the microstructure of the $\text{Cu}_{1.6}\text{Mn}_{1.4}\text{Al}$ (Cu-35.1at.%Mn-25.1at.%Al) alloy was a mixture of ($L2_1 + B2 + L\text{-}J$) phases. This is different from that observed by previous workers in the $\text{Cu}_{3-x}\text{Mn}_x\text{Al}$ alloys with $X \leq 1.0$. When the as-quenched alloy was aged at 460°C for short times, γ -brass precipitates started to occur at APBs. After prolonged aging time at 460°C , the γ -brass precipitates grew and β -Mn precipitates generated at the regions contiguous to the γ -brass precipitates. The orientation relationship between the γ -brass and β -Mn was $(001)_{\gamma\text{-brass}} // (012)_{\beta\text{-Mn}}$ and $(011)_{\gamma\text{-brass}} // (031)_{\beta\text{-Mn}}$. The coexistence of (γ -brass + β -Mn) has never been observed by previous workers in Cu-Mn-Al alloy systems before. When the as-quenched alloy was aged at temperatures ranging from 460°C to 700°C , the phase transition sequence was found to be $(\gamma\text{-brass} + \beta\text{-Mn}) \rightarrow (\beta\text{-Mn} + B2) \rightarrow \beta$.

Contents

	<u>page</u>
中文摘要	i
Abstract	iv
Contents	vii
List of Tables	ix
List of Figures	x
Chapter 1. General Introduction.....	錯誤! 尚未定義書籤。
Chapter 2. As-quenched Microstructures of $\text{Cu}_{3-x}\text{Mn}_x\text{Al}$ Alloys	15
2-1 Introduction.....	17
2-2 Experimental procedure.....	19
2-3 Results and discussion.....	21
2-4 Conclusions.....	43
References.....	45
Chapter 3. Phase Transformations in a $\text{Cu}_{2.7}\text{Mn}_{0.3}\text{Al}$ Alloy.....	47
3-1 Introduction.....	49
3-2 Experimental procedure.....	51
3-3 Results and discussion.....	52
3-4 Conclusions.....	74
References.....	75
Chapter 4. Phase Transformations in a $\text{Cu}_{1.6}\text{Mn}_{1.4}\text{Al}$ Alloy	77
4-1 Introduction.....	79
4-2 Experimental procedure.....	81
4-3 Results.....	82
4-4 Discussion.....	101

4-5 Conclusion	107
References.....	109
Chapter 5. Summary	111
List of Publications	115



List of Tables

Table 2.1 Atomic and Chemical compositions of the present alloys by inductively coupled plasma-mass spectrometer (ICP).....	20
Table 3.1 Chemical Compositions of the Phases Revealed by an Energy-Dispersive X-ray Spectrometer (EDS)	73
Table 4.1 Chemical Compositions of the Phases Revealed by an Energy-Dispersive X-ray Spectrometer (EDS).....	104



List of Figures

- Figure 1.1 A schematic drawing of the phase diagram of the Cu-Al alloy system with A2 \rightarrow B2 and B2 \rightarrow D0₃ order-disorder transition temperatures and martensitic transformation temperatures (Ms) [6-7]..... 12
- Figure 1.2 A schematic drawing of the ordering temperatures T_c (B2) and T_c (D0₃ + L2₁) and the miscibility gap of the (Cu-Mn)₃Al alloy [25].13
- Figure 1.3 Schematic representation of the ordering sequence of the quenched Cu_{2.5}Mn_{0.5}Al alloy (vertically) and its isothermal decomposition (horizontally) [19, 25, 39]..... 14
- Figure 2.1 Influence of Manganese concentration on the microstructures of Cu-Mn-Al alloys. (a) Cu_{2.9}Mn_{0.1}Al (b) Cu_{2.8}Mn_{0.2}Al (c) Cu_{2.7}Mn_{0.3}Al (d) Cu_{2.6}Mn_{0.4}Al. 23
- Figure 2.2 Electron micrographs of the as-quenched Cu_{2.9}Mn_{0.1}Al alloy. (a) BF, (b) through (c) three SADPs. The zone axes of the D0₃ phase, γ_1' martensite and internal twin are (b) [001], [10 $\bar{1}$] and [$\bar{1}$ 01], (c) [011], [1 $\bar{1}$ $\bar{1}$] and [$\bar{1}$ 00] (d) [111], [01 $\bar{2}$] and [$\bar{2}$ 10], respectively (\underline{hkl} = D0₃ phase, hkl= γ_1' martensite, hkl_T=internal twin). (e) and (f) (1 $\bar{1}$ 1) and (200) D0₃ DF, respectively, (g) (1 $\bar{2}$ 1) γ_1' DF..... 28
- Figure 2.3 Electron micrographs of the as-quenched Cu_{2.8}Mn_{0.2}Al alloy. (a) BF, (b) through (d) three SADPs. The zone axes of the D0₃ phase

are [100], [110] and [111], respectively (\underline{hkl} = D0₃ phase, hkl_{1or2} = L-J phase, 1: variant 1; 2: variant 2). (e) and (f) ($\bar{1}11$) and (002) D0₃ DF, respectively, (g) (100₁) L-J DF..... 32

Figure 2.4 Electron micrographs of the as-quenched Cu_{2.7}Mn_{0.3}Al alloy. (a) BF, (b) and (c) two SADPs. The zone axes of the D0₃ phase are [100] and [110], respectively. (\underline{hkl} = D0₃ phase, hkl_{1or2} = L-J phase, 1: variant 1; 2: variant 2). (d) and (e) ($\bar{1}11$) and (002) D0₃ DF, respectively. (f) (100₁) L-J DF..... 36

Figure 2.5 Electron micrographs of the as-quenched Cu_{2.6}Mn_{0.4}Al alloy. (a) BF, (b) and (c) two SADPs. The zone axes of the D0₃ phase are [100] and [110], respectively. (\underline{hkl} = (D0₃ + L2₁) phase, hkl_{1or2} = L-J phase, 1: variant 1; 2: variant 2). (d) and (e) ($\bar{1}11$) and (002) D0₃ DF, respectively, (f) (100₁) L-J DF..... 40

Figure 3.1 Electron micrographs of the as-quenched alloy. (a) BF, (b) and (c) two SADPs. The zone axes of the D0₃ phase are (b) [100] and (c) [110], respectively (\underline{hkl} = D0₃, $hkl_{1,2}$ = L-J phase, 1: variant 1; 2:variant 2), (d) and (e) ($\bar{1}11$) and (002) D0₃ DF, respectively. (f) (0 $\bar{2}0_1$) L-J DF..... 55

Figure 3.2 Electron micrographs of the alloy aged at 500 °C for 20 minutes. (a) BF, (b) and (c) two SADPs. The zone axes of the D0₃ phase is [100] and [110], respectively. (\underline{hkl} =D0₃, hkl_1 =L-J phase and hkl_2 = γ -brass), (c) and (d) ($\bar{1}11$) D0₃ and (100₁) L-J DF, respectively.

(f) (100) γ -brass DF..... 59

Figure 3.3 Electron micrographs of the alloy aged at 500°C for 2 hours. (a) BF, (b) and (c) two SADPs. The zone axes of the $D0_3$ phase are [100] and [110]. ($hkl=D0_3$, $hkl_1=L$ -J phase and $hkl=\gamma$ -brass), respectively. (d) and (e) (100_1) L-J and $(\bar{1}11)$ $D0_3$ DF, respectively. 62

Figure 3.4 Electron micrographs of the alloy aged at 600 °C for 1 hour. (a) BF, (b) an SADP taken from the irregular-shaped γ -brass particle. The zone axis of the γ -brass phase is [001]. (c) an SADP taken from the $D0_3$ matrix. The zone axis of the $D0_3$ phase is [110]. ($hkl=D0_3$, $hkl_1=L$ -J phase). (d) $(0\bar{2}0_1)$ L-J DF. (e) and (f) $(\bar{1}11)$ and (002) $D0_3$ DF, respectively..... 66

Figure 3.5 Electron micrographs of the alloy aged at 700 °C for 1 hour. (a) and (b) $(\bar{1}11)$ and (002) $D0_3$ DF, respectively. 68

Figure 3.6 Three typical EDS spectra obtained from (a) as-quenched alloy, (b) a γ -brass particle, and (c) an L-J precipitate in the alloy aged at 500°C for 2 hours, respectively..... 72

Figure 4.1 Electron micrographs of the as-quenched alloy. (a) BF, (b) through (c) two SADPs. The zone axes of the $L2_1$ phase are [100] and [110], respectively ($hkl=L2_1$, $hkl_{1,2}=L$ -J phase, 1:variant 1; 2:variant 2). (d) and (e) $(\bar{1}11)$ and (002) $L2_1$ DF, respectively. (f) (100_1) L-J DF. 85

Figure 4.2 Electron micrographs of the alloy aged at 460°C for 10 minutes.
(a) and (b) $(\bar{1}11)$ and (002) $L2_1$ DF, respectively. (c) (100_1) L-J DF.
..... 88

Figure 4.3 Electron micrographs of the alloy aged at 460°C for 30 minutes.
(a) (002) $L2_1$ DF, (b) and (c) two SADPs. The zone axes of the $L2_1$
phase is $[100]$ and $[110]$. ($hkl = L2_1$, $hkl = \gamma$ -brass). 90

Figure 4.4 Electron micrographs of the alloy aged at 460°C for 6 hours. (a)
BF, (b) and (c) two SADPs. The zone axes of the β -Mn are $[001]$
and $[011]$. (d) and (e) two SADPs. The zone axes of the γ -brass
are $[001]$ and $[011]$. (f) an SADP. The zone axis of the β -Mn and
the γ -brass is $[100]$ and $[100]$, respectively. ($hkl = \beta$ -Mn,
 $hkl = \gamma$ -brass). 93

Figure 4.5 BF electron micrograph of the alloy aged at 460°C for 12 hours.
..... 96

Figure 4.6 Electron micrographs of the alloy aged at 600°C for 30 minutes.
(a) BF, (b) and (c) two SADPs. The zone axes are $[20\bar{1}]_{\beta\text{-Mn}}$,
 $[100]_{\beta\text{-Mn}}$ for the β -Mn and $[100]_{L2_1}$, $[201]_{L2_1}$ for the $L2_1$ matrix,
respectively. ($hkl = \beta$ -Mn, $hkl_1 = L$ -J phase, $hkl = \gamma$ -brass). (d) and (e)
 $(\bar{1}11)$ and (002) $L2_1$ DF, respectively. (f) (100_1) L-J DF. 99

Figure 4.7 Electron micrographs of the alloy aged at 700°C for 1 hour. (a)
and (b) $(\bar{1}11)$ and (002) $L2_1$ DF, respectively. 100

Figure 4.8 Three typical EDS spectra obtained from (a) as-quenched alloy,

(b) a γ -brass precipitate as well as (c) a β -Mn precipitate in the alloy aged at 460°C for 6 hours. 103

